Supplementary Information

Aromatic amine electrochemical sensors based on a Co-MOF: a hydrogen bond-induced specific response

Xiao-qin Wu, Ze-yu Yang, Xiao-jie Sang, Xin-xin Tian* and Xuehong Wei*

1. Chemicals and Instrumentation

Hexahydrate cobalt nitrate (II) (Co(NO$_3$)$_2$·6H2O), 2,5-thiophene dicarboxylic acid (H$_2$L), 2,2-bipyridine (bipy), 1, 3-dinitrobenzene(m-DNB), 2, 4-dinitroaniline (2, 4-DNA), 4-nitro-o-phenylenediamine(4-NOPD), p-nitroaniline(p-NA)   and N,N-dimethyl acetamide (DMA) were commercially available and used directly as provided without further purification.

The powder X-ray diffraction (PXRD) patterns were collected by a D/Max-2500 Advance X-ray diffractometer (Bruker, Germany) from 5° to 50°. Thermogravimetric analysis (TGA) was carried out in the temperature range of 50–800 °C at a heating rate of 10 °C min^{-1} in an air atmosphere with a flow rate of 30 mL min^{-1} using a NETZSCH TG 209 (Netzsch instruments, Germany). The Fourier Transform Infrared Spectrometer spectra (FTIR) were obtained with a Bruker Tensor 27 infrared micro-spectrometer (Bruker, Germany).

2. X-ray crystallography

The X-ray single crystal diffractiondata were collected with a Bruke D8 Venture diffractometer (Bruker,Germany) at room temperature (real-time temperature 301 K) using graphite monochromatic Mo Kα radiation (λ = 0.71073 Å). The structures were solved by SHELXT (direct methods) and refined by SHELXL (full matrix least-squares techniques)[1] in the Olex2 package.[2]

Table S1. Crystal data and structure refinements for **Co-1**

Co-1(CCDC number: 2246519)	
formula	$C_{22}H_{16}Co_2N_2O_{10}S_2$
M, g mol^{-1}	650.35
crystsyst	Triclinic system
space group	P-1
a / Å	11.1342(4)
b / Å	11.1512(4)
c / Å	15.5072(6)
α / deg	84.2880(10)
β / deg	87.7790(10)
γ / deg	86.1610(10)
V / Å^3	1910.51(12)
Z	2
reflns collected	22961
Unique reflns	6719
$R1$ [I > 2σ(I)]	0.0442
wR_2(all data)	0.1419

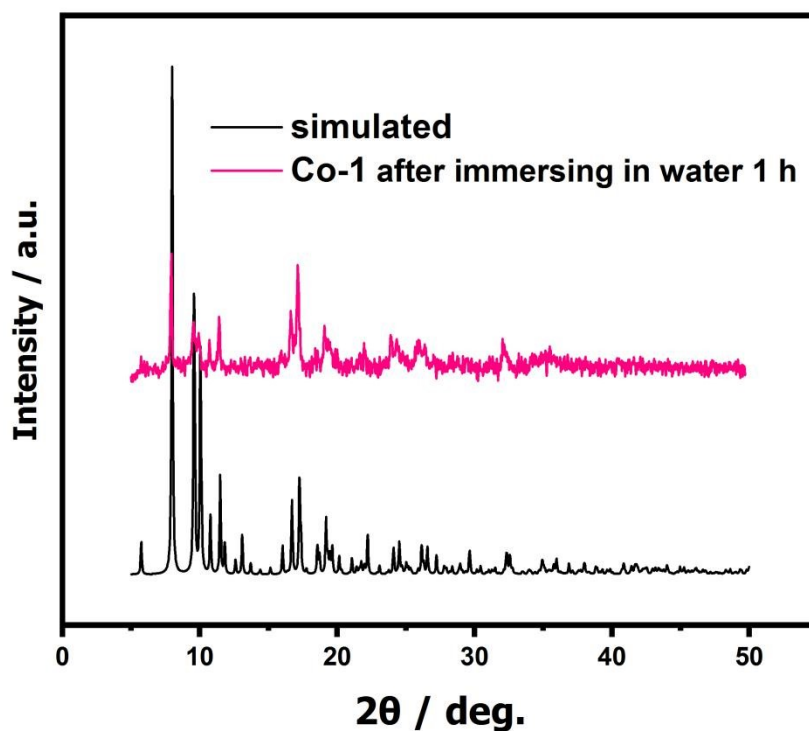**3. PXRD test of Co-1 after immersing in water 1 h**

Fig. S1. PXRD graphs of **Co-1** simulated by the single crystal data or after immersing in water for 1 h.

4. Thermo gravimetric analysis (TGA)

TGA results show that the weight loss of about 3% observed between 0-100℃ was ascribed to volatilization of two water molecule and the weight loss of 19.7% observed between 100-200℃ was ascribed to volatilization of one DMA molecule in the lattice. When the temperature in the range from 200 to 300℃, the curve is in the platform stage, indicating that **Co-1** can exist stably in this temperature range and when the temperature reaches 350℃, the curve drops sharply, **Co-1** crystals begin to decompose.
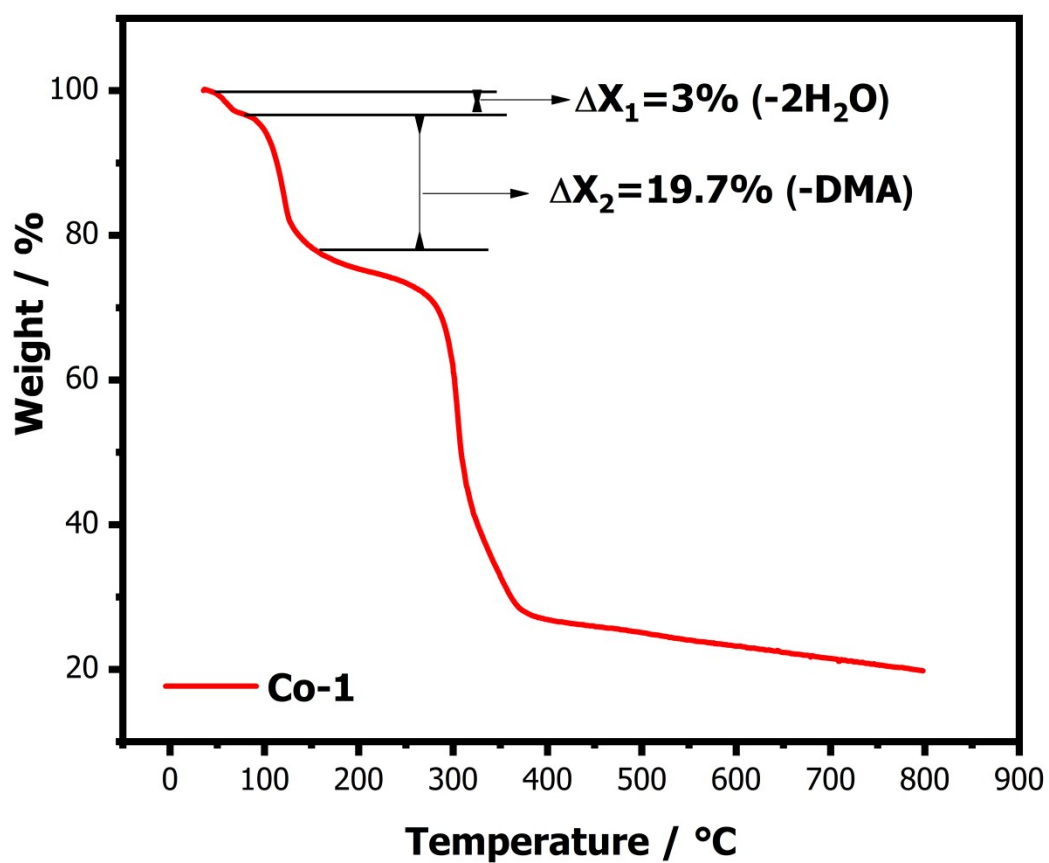
Fig. S2. TGA graphs of **Co-1**
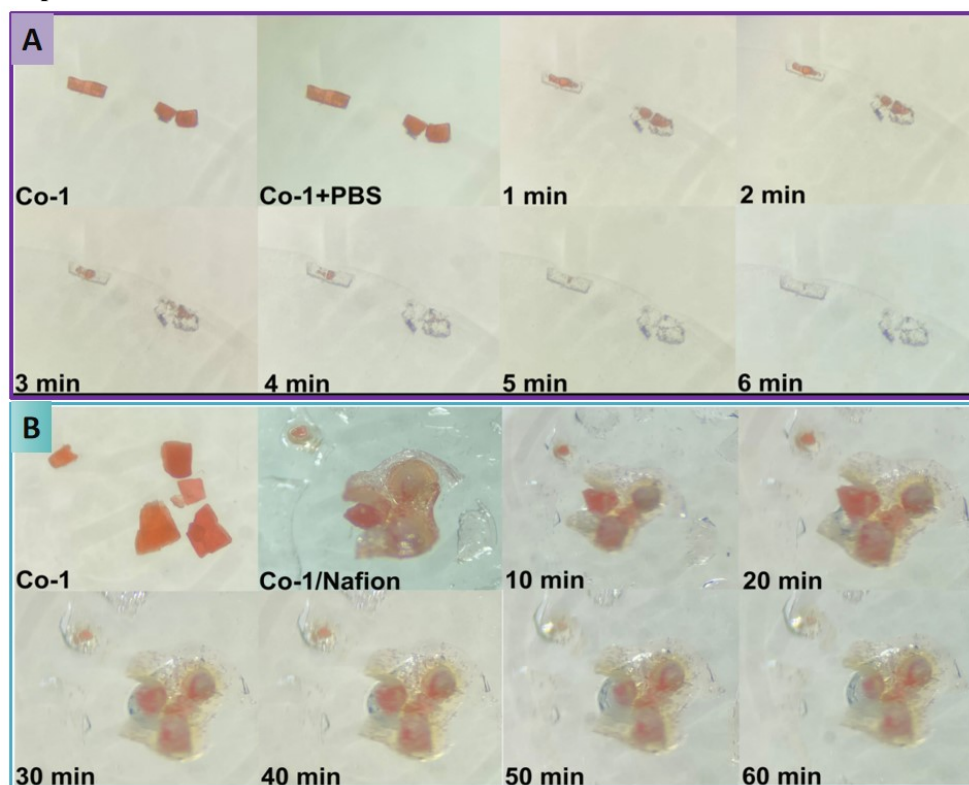
5. The protective effect of nafion on Co-1

Fig. S3. (A) the microscopic pictures of **Co-1** immersed in phosphate buffer solution (pH=6.8) for six minutes; (B) the microscopic pictures of **Co-1**/nafion immersed in phosphate buffer solution (pH=6.8) for one hour.
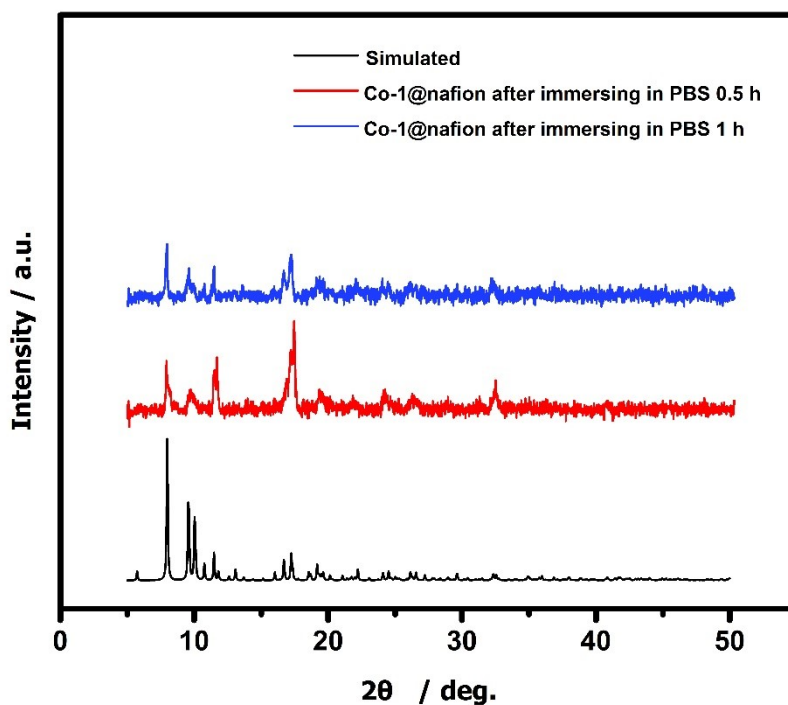

Fig. S4. PXRD graphs of **Co-1** simulated by the single crystal data or after immersing in PBS for 0.5 h, 1 h.

6. The Fourier Transform Infrared Spectrometer (FTIR) spectra

The FT-IR spectra of Co-1 (KBr, cm^{-1}): 671(m), 772(s), 797(m), 839(m), 888(w), 965(w), 1015(w), 1077(w), 1106(m), 1158(w), 1224(w), 1252(w), 1358(s), 1389(s), 1435(w), 1508(w), 1576(s), 1610(s), 1654(m); The FT-IR spectra of 2,2-bipy (KBr, cm^{-1})：653(m), 750(s), 894(w), 992(m), 1040(m), 1063(w), 1084(m), 1139(w), 1212(w), 1251(m), 1416(m), 1450(m), 1557(m), 1578(m); The FT-IR spectra of H2L (KBr, cm^{-1}):681(w), 750(w), 850(m), 914(m), 1038(m), 1101(w), 1229(m), 1260(m), 1340(w), 1412(m), 1525(m), 1658(m).
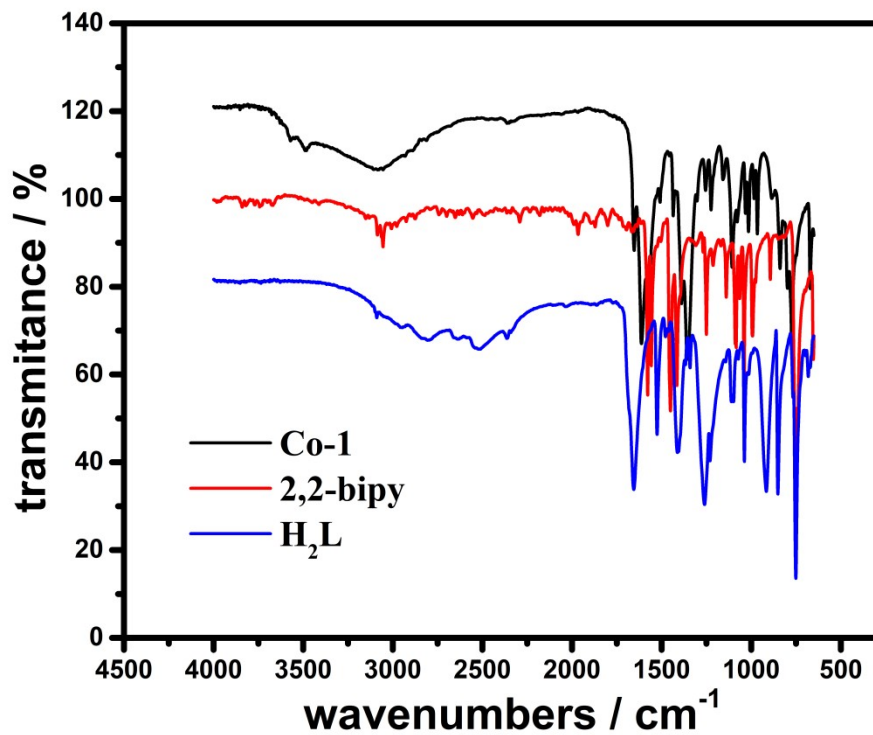

Fig. S5. The FT-IR spectra of **Co-1**, 2,2-bipy and H$_2$L.

7. Electrochemical Section of Co-1/GCE

A CHI660e electrochemical workstation (Chenhua Instrument, Shanghai, China) was used for electrochemical measurements with a three-electrode system: the working electrode was the bare glassy carbon electrode (GCE) or **Co-1** modified GCE, **Co-1**/GCE. The counter electrode was a platinum wire and the reference electrode was an $Hg/HgCl_2/KCl$ electrode. Electrolyte: Phosphoric acid buffer solution (PBS, pH=6.86); All electrochemical studies were carried out at room temperature and under nitrogen surroundings.
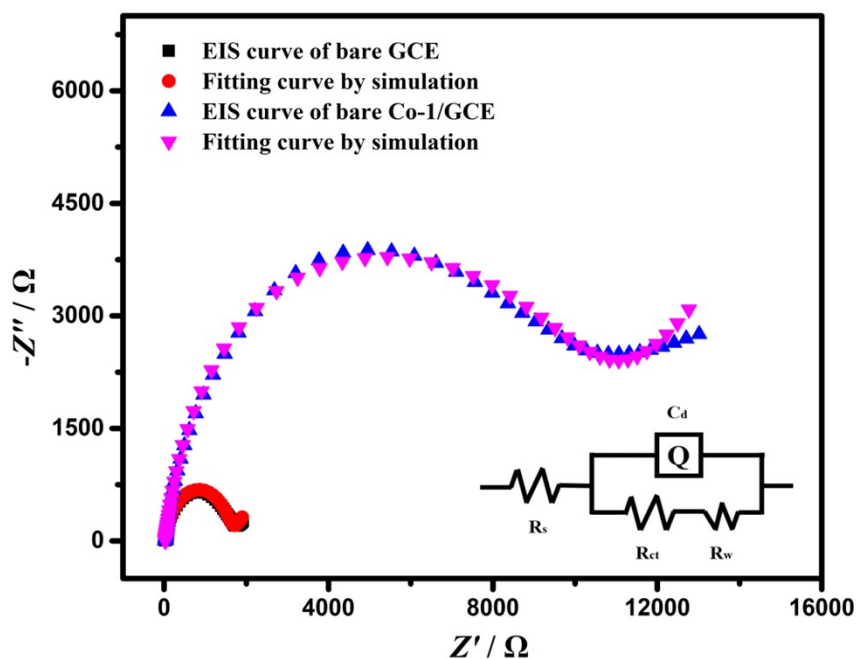

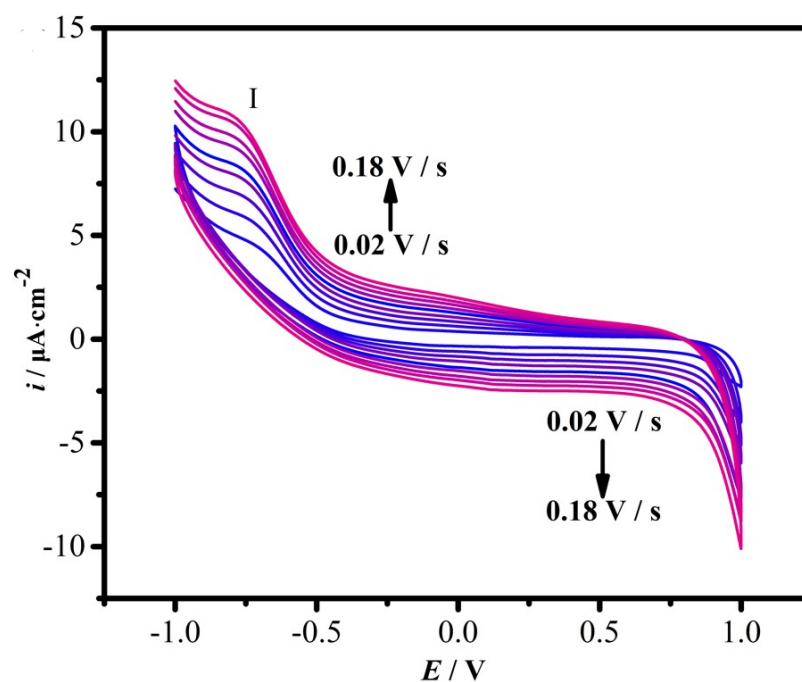Fig. S6. Nyquist plots of impedance spectra as the bare GCE and **Co-1**/GCE.

Fig. S7. CVs at **Co-1**/GCE with different scan rates in the range from 0.02 V/s ~ 0.18 V/s.
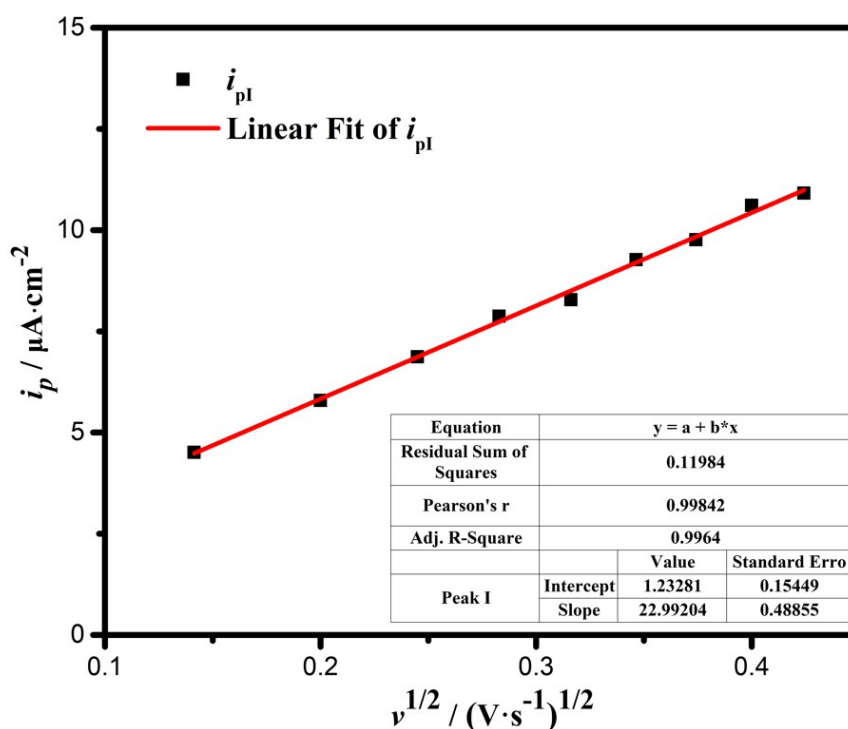
Fig. S8. Plots and parameters of $i_{p,I}$ vs square root of scan rates $v^{1/2}$.

8. Methods and Model of DFT calculations

Spin-polarized and periodic density functional theory (DFT) calculations were carried out with the Vienna *ab initio* simulation package (VASP)[3,4]. The generalized gradient approximation in the Perdew-Burke-Ernzerhof (GGA-PBE) functional[5,6] was used to treat the electron exchange and correlation energies. The dispersion interactions (D3 correction) were included in the geometry optimization.[7] The cut off energy was set up to 400 eV. The convergence criterion of force and energy for the geometry optimization was 0.02 eV/Å, 10^{-4} eV, respectively.

The MOF cell was obtained by experimental characterization and optimized using $3 \times 3 \times 2$ Monkhorst–Pack k-point sampling. The lattice constant is a = 11.1342 Å, b = 11.1512 Å, c = 15.5072 Å, α = 84.288 º, β = 87.779 º, γ = 86.161º. All atoms were allowed to relax.

The adsorption energy (E_{ads}) of guest molecule (A) is calculated using $E_{ads} = E(A/MOF) - E(A) - E(MOF)$, where $E(A/MOF)$ is the total energy of the MOF model with guest molecule A in its equilibrium geometry, $E(A)$ is the total energy of the guest molecule in gas phase, $E(MOF)$ is the total energy of the used MOF cell.

2,4-DNA-3 (-0.90 eV)
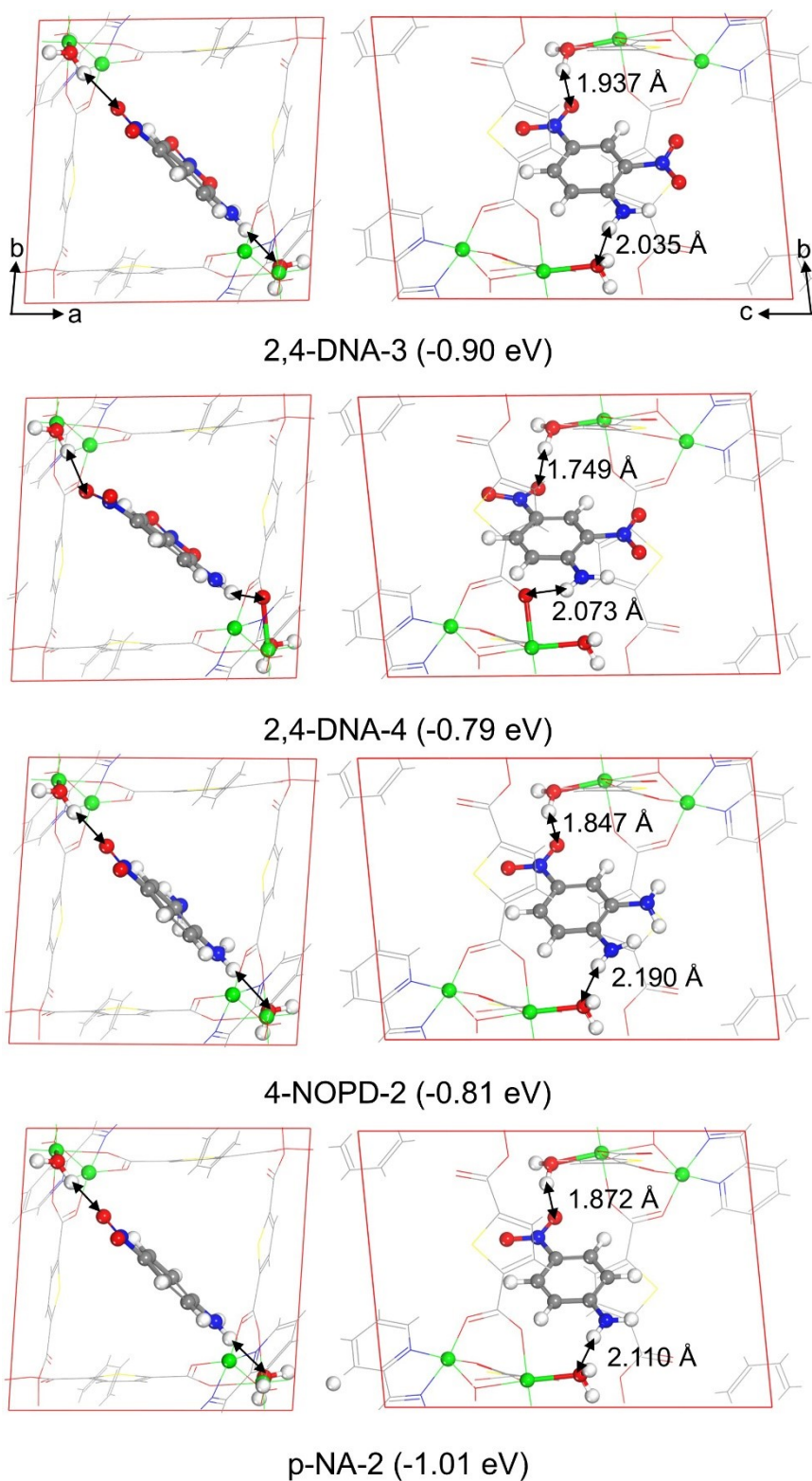
2,4-DNA-4 (-0.79 eV)

4-NOPD-2 (-0.81 eV)

p-NA-2 (-1.01 eV)

Fig. S9. The structures of 2,4-DNA, 4-NOPD and p-NA interacting with **Co-1** skeleton through both NO_2 and NH_2 group (view from different direction).

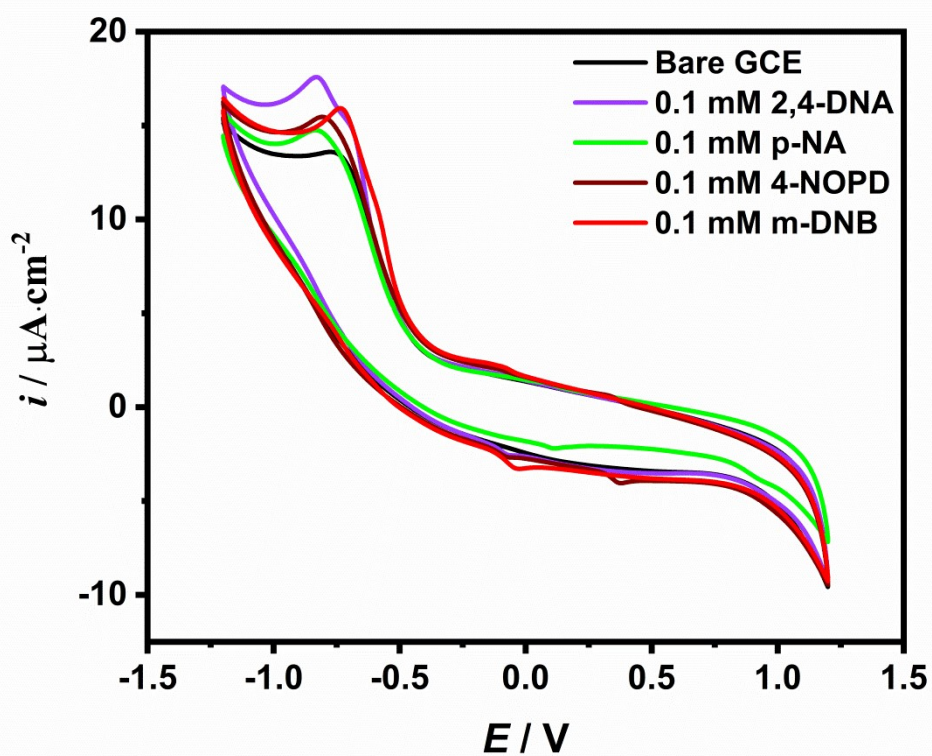9. **Electrochemical Sensing behaviors of Co-1/GCE**

Fig. S10. CVs of bare GCE in PBS solution with 0.1 mM 2.4-DNA, 0.1 mM p-NA, 0.1 mM 4-NOPD or 0.1 mM m-DNB.
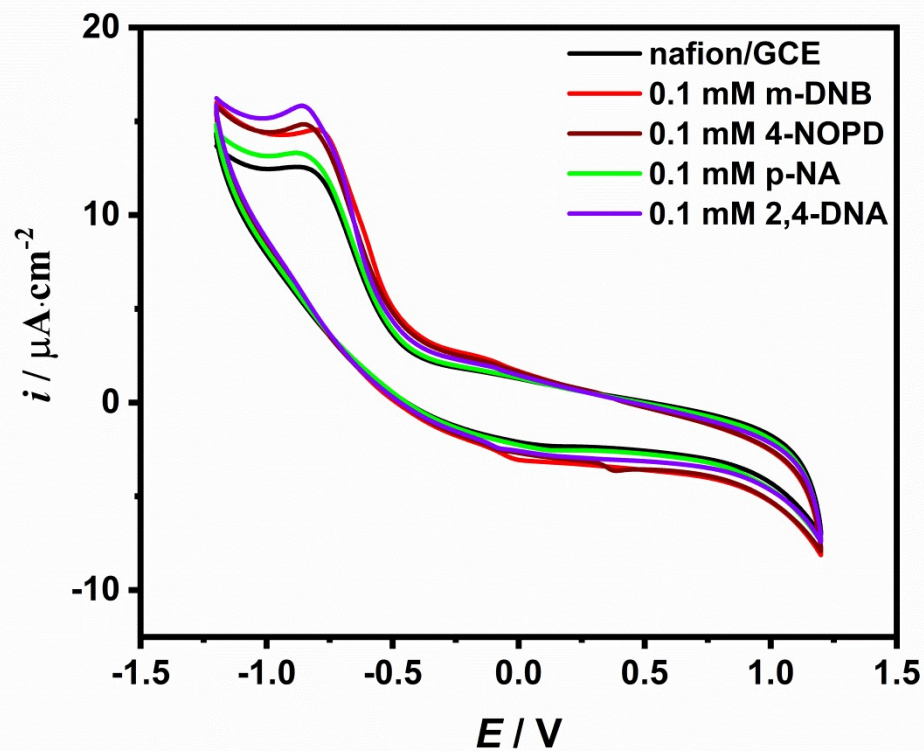

Fig. S11. CVs of Nafion/GCE in PBS solution with 0.1 mM 2.4-DNA, 0.1 mM p-NA, 0.1 mM 4-NOPD or 0.1 mM m-DNB.
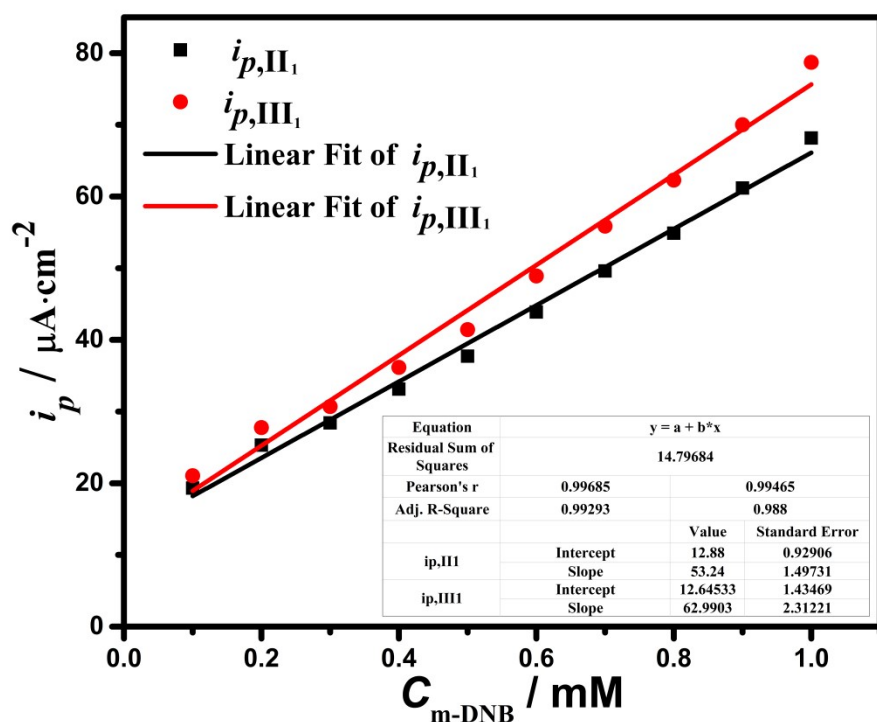
Fig. S12 table

Equation		y = a + b*x	
Residual Sum of Squares		14.79684	
Pearson's r	0.99685	0.99465	
Adj. R-Square	0.99293	0.988	
		Value	Standard Error
ip,II1	Intercept	12.88	0.92906
	Slope	53.24	1.49731
ip,III1	Intercept	12.64533	1.43469
	Slope	62.9903	2.31221

Fig. S12. The calibration plot of current intensities $i_{p,II1}$ and $i_{p,III1}$ vs the different concentrations of m-DNB from 0.1~1.0 mM.

Fig. S13 table

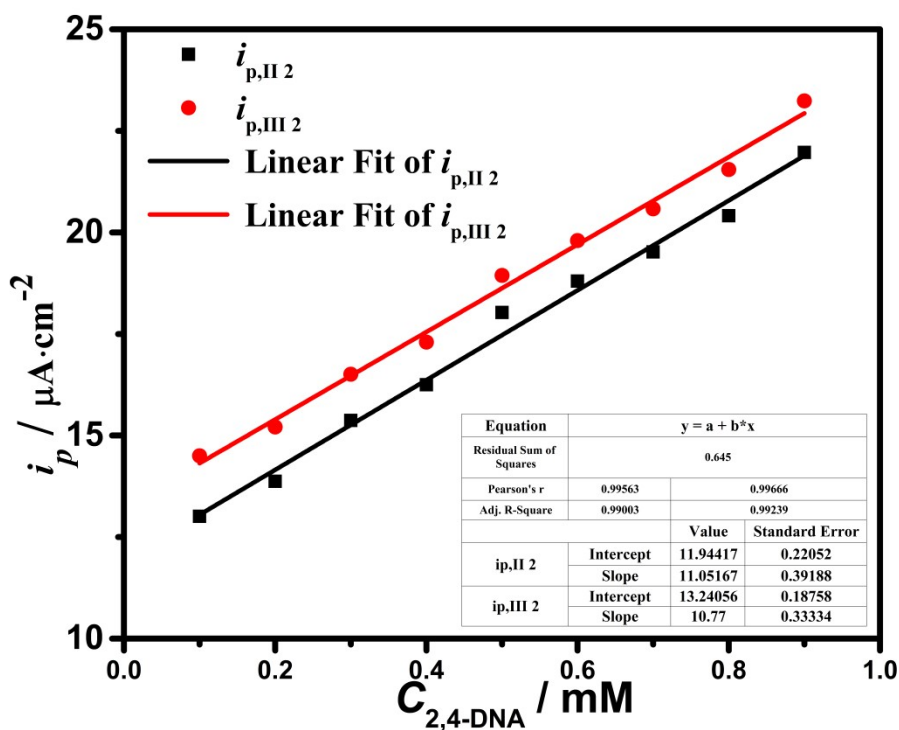| Equation		y = a + b*x	
Residual Sum of Squares		0.645	
Pearson's r	0.99563	0.99666	
Adj. R-Square	0.99003	0.99239	
		Value	Standard Error
ip,II 2	Intercept	11.94417	0.22052
	Slope	11.05167	0.39188
ip,III 2	Intercept	13.24056	0.18758
	Slope	10.77	0.33334

Fig. S13. The calibration plot of current intensities $i_{p,II2}$ and $i_{p,III2}$ vs the different concentrations of 2,4-dinitroaniline from 0. 1~0.9 mM.
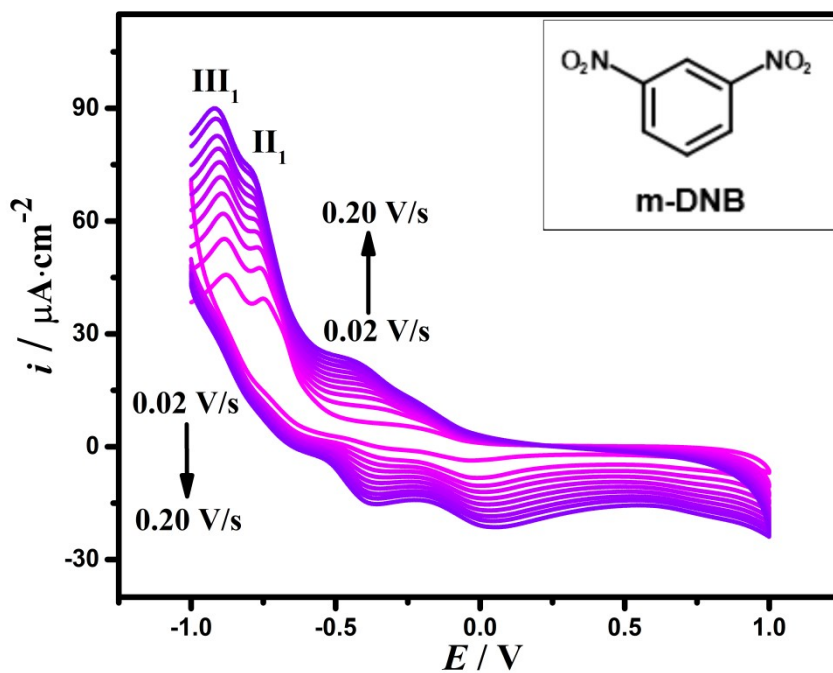
Fig. S14. CVs at **Co-1**/GCE in PBS (pH=6.86) containing 1.0 mM m-DNB at different scan rates from 0.02 to 0.2 V·s^{-1};
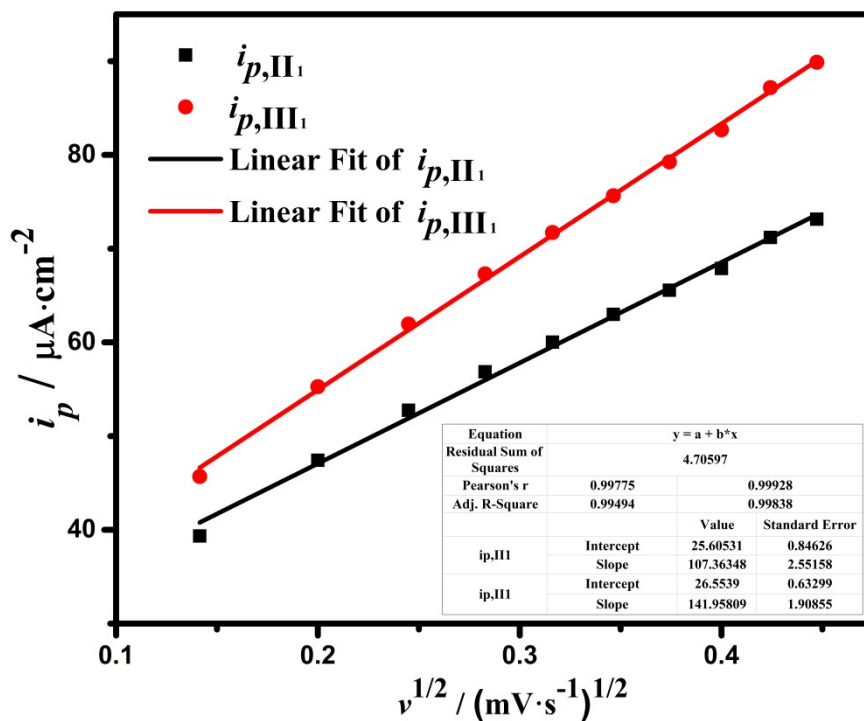

Fig. S15. The calibration plot of current intensities $i_{p,II1}$ and $i_{p,III1}$ vs the square root of scan rate $v^{1/2}$.
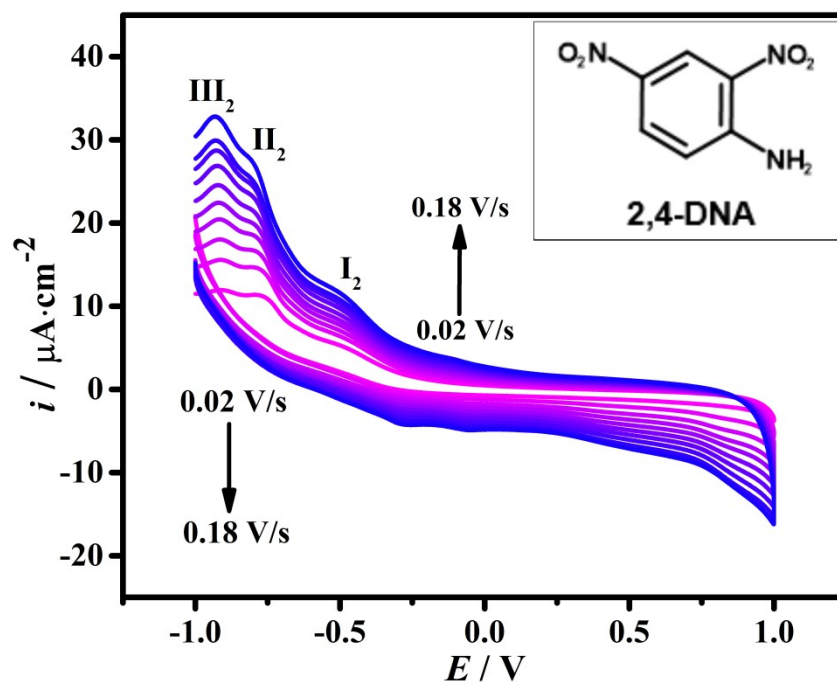
Fig. S16. CVs at **Co-1**/GCE in PBS (pH=6.86) containing 0.9 mM 2,4-DNA at different scan rates from 0.02 to 0.2 V·s^{-1};

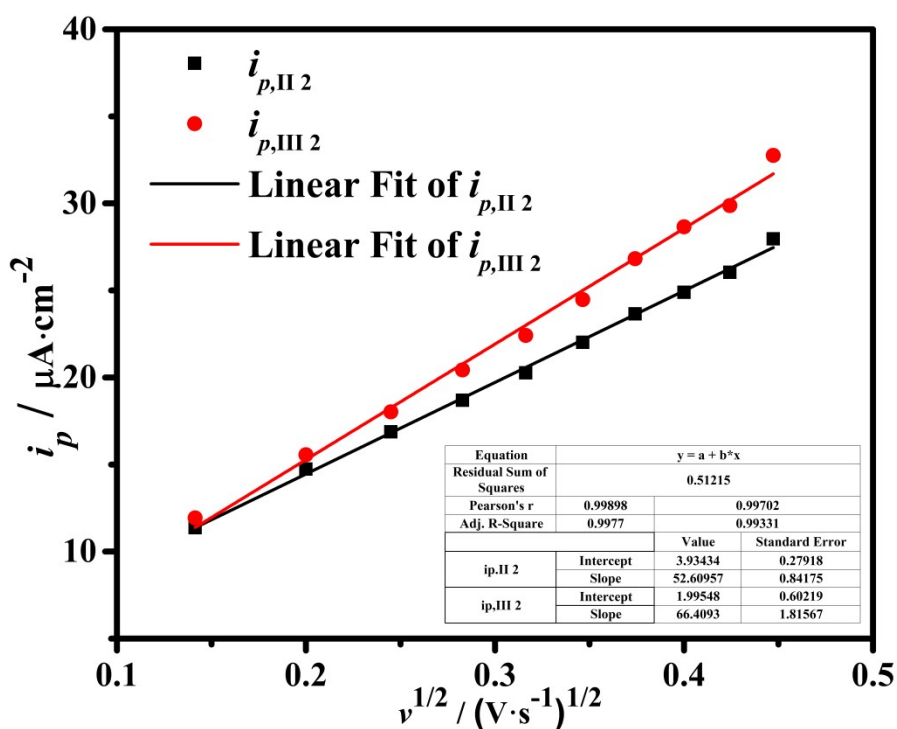| Equation		y = a + b*x	
Residual Sum of Squares		0.51215	
Pearson's r	0.99898	0.99702	
Adj. R-Square	0.9977	0.99331	
		Value	Standard Error
ip,II 2	Intercept	3.93434	0.27918
	Slope	52.60957	0.84175
ip,III 2	Intercept	1.99548	0.60219
	Slope	66.4093	1.81567

Fig. S17. The calibration plot of current intensities $i_{p,II2}$ and $i_{p,III2}$ vs the square root of scan rate $v^{1/2}$.
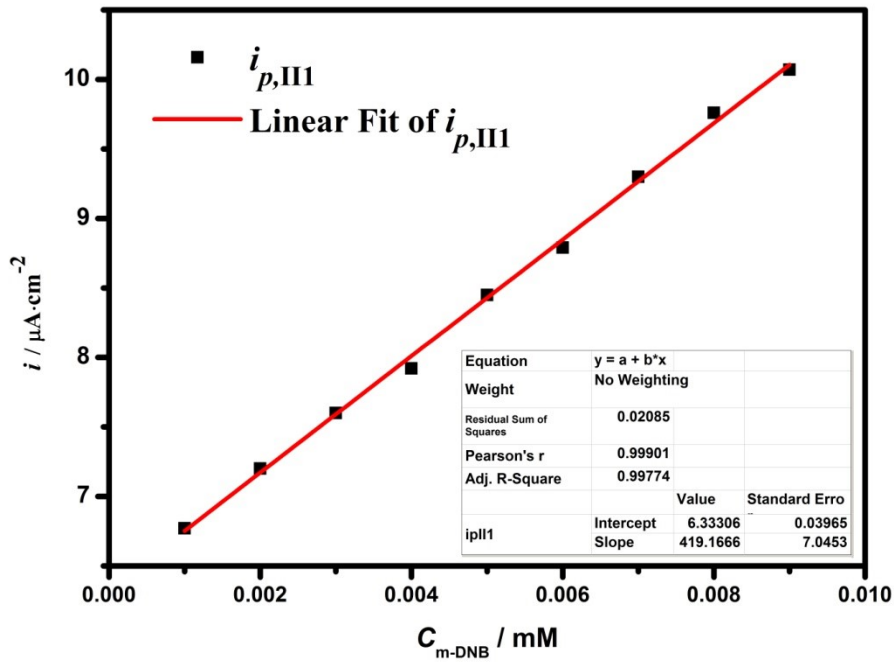
Fig. S18. The calibration plot of current intensities $i_{p,II1}$ vs the concentration of m-DNB based on DPV curve.
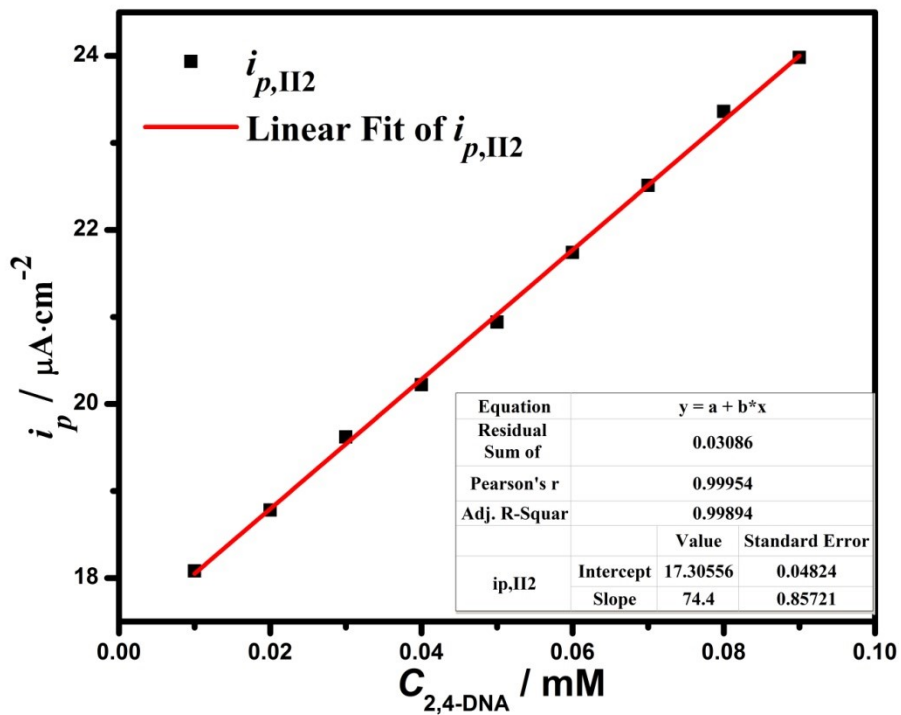

Fig. S19. The calibration plot of current intensities $i_{p,II2}$ vs the concentration of 2,4-DNA based on DPV curve.
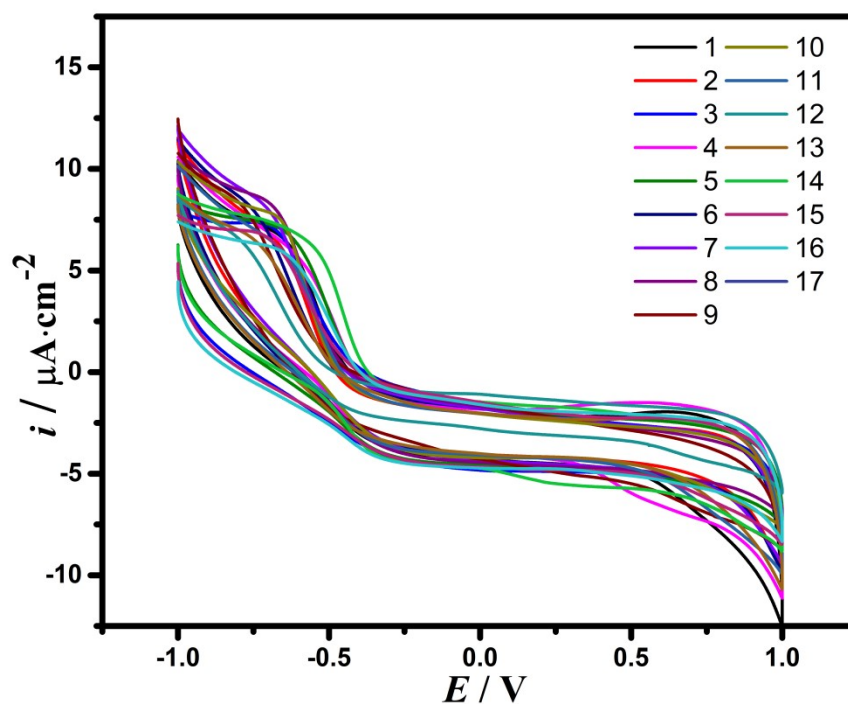
Fig. S20. CVs of **Co-1**/GCE in PBS solution with 0.1 mM different interferents (1-17): **1.** benzamide; **2.** β-naphthylamine; **3.** α-naphthylamine; **4.** 2-nitrobenzaldehyde; **5.** 3-nitrobenzaldehyde; **6.** 4-nitrobenzaldehyde; **7.** 2-nitrobenzoic acid; **8.** 3-nitrobenzoic acid; **9.** 4-methylbenzyl alcohol; **10.** 2-acetylpyridine; **11.** benzonitrile; **12.** 4-aminobenzoic acid; **13.** phthalic acid; **14.** 2-chlorobenzaldehyde; **15.** aniline; **16.** 2,4,6-trimethylaniline; **17.** benzene-1,3-diamine.

Fig. S21. CVs of **Co-1**/GCE in PBS solution with 0.5 mM m-DNB containing 0.1 mM different interferents (1-17): **1.** benzamide; **2.** β-naphthylamine; **3.** α-naphthylamine; **4.** 2-nitrobenzaldehyde; **5.** 3-nitrobenzaldehyde; **6.** 4-nitrobenzaldehyde; **7.** 2-nitrobenzoic acid; **8.** 3-nitrobenzoic acid; **9.** 4-methylbenzyl alcohol; **10.** 2-acetylpyridine; **11.** benzonitrile; **12.** 4-aminobenzoic acid; **13.** phthalic acid; **14.** 2-chlorobenzaldehyde; **15.** aniline; **16.** 2,4,6-trimethylaniline; **17.** benzene-1,3-diamine.
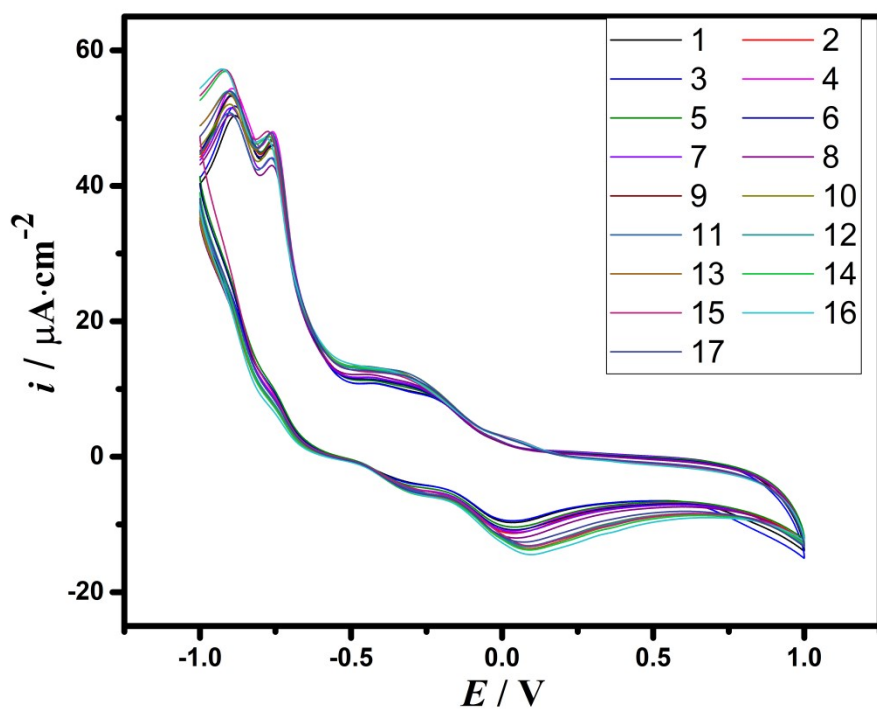
Fig. S22. CVs of **Co-1**/GCE in PBS solution with 0.5 mM 2,4-DNA containing 0.1 mM different interferents (1-17): **1.** benzamide; **2.** β-naphthylamine; **3.** α-naphthylamine; **4.** 2-nitrobenzaldehyde; **5.** 3-nitrobenzaldehyde; **6.** 4-nitrobenzaldehyde; **7.** 2-nitrobenzoic acid; **8.** 3-nitrobenzoic acid; **9.** 4-methylbenzyl alcohol; **10.** 2-acetylpyridine; **11.** benzonitrile; **12.** 4-aminobenzoic acid; **13.** phthalic acid; **14.** 2-chlorobenzaldehyde; **15.** aniline; **16.** 2,4,6-trimethylaniline; **17.** benzene-1,3-diamine.
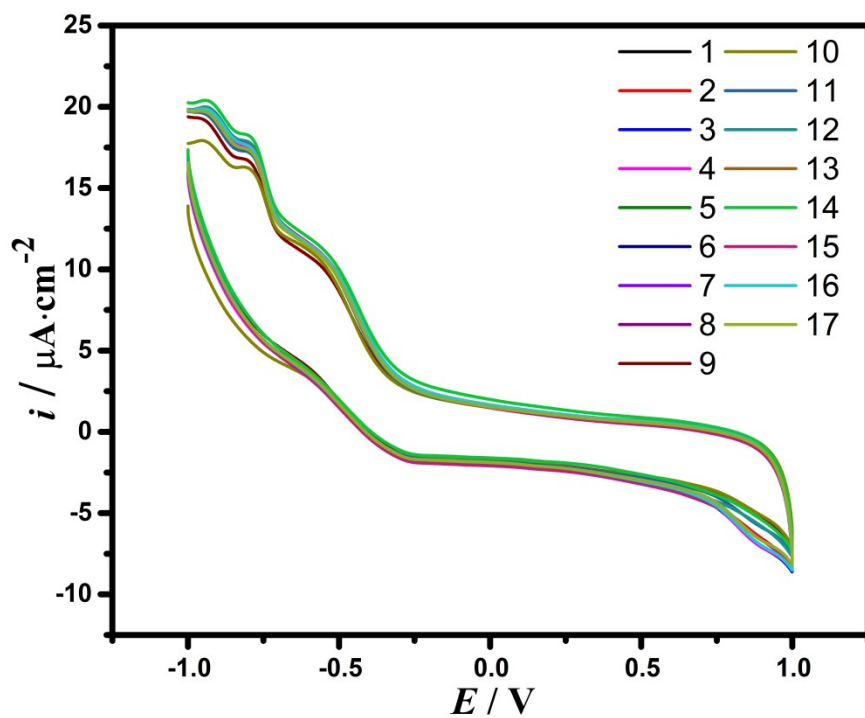
10. Comparison of different detection methods in the recognition efficiency of m-DNB

Table S2. Comparison of different detection methods in the recognition efficiency of m-DNB

Method/materials	Detection range	LOD	Ref
Colorimetric aqueous medium dual chemosensor	0.5–5.0 μL	0.084 ppb	8
Photoluminescent sensor	0-100 ppm	6.109 ppm	9
Tb-MOF sensor	8-240 μM	1.89 μM	10
Cu-MOF Fluorescence sensor	25-45 ppb	0.7544 ppb	11
Electrochemical sensor/Co-MOF	0.01 mM-0.09 mM	0.0286 μM	This work

Note after first publication

This electronic supplementary information replaces the version published on 17th October 2022, which contained errors in the crystallographic data and the test temperature of X-ray single crystal diffraction for **Co-1**.

[1] G. Sheldrick, *ActaCryst.* 2008**, 64 (1)**, 112-122.

[2] O. V. Dolomanov, L. J. Bourhis, R. J. Gildea, J. A. K. Howard and H. Puschmann, *J. Appl. Cryst.* 2009**, 42 (2)**, 339-341.

[3] G. Kresse and J. Furthmueller, *Comput. Mater. Sci.* 1996, **6**, 15-50.

[4] G. Kresse and J. Furthmueller, *Phys. Rev. B* 1996, **54**, 11169-11186.

[5] J. P. Perdew, K. Burke and M. Ernzerhof, *Phys. Rev. Lett.* 1997, **78**, 1396.

[6] J. P. Perdew, K. Burke and M. Ernzerhof, *Phys. Rev. Lett.* 1996, **77**, 3865-3868.

[7] S. Grimme, J. Antony, S. Ehrlich and H. Krieg, *J. Chem. Phys.* 2010, **132**, 154104.

[8] S. Shakya, I. M. Khan and M. Ahmad, *J. Photoch. Photobio. A* 2020, **92**, 112402.

[9] L.Tashi, R. Singhaal, M. Kumar and H. N. Sheikh, *New J. Chem.* 2020*, 44*, 19908-19923.

[10] J. F. Guo, M. Y. Zhang, Q. Z. Guo, G. P. Yan and L. J. Liu, *Inorg. Chim. Acta*, 2021, **525**, 120454.

[11] D. Garg, H. Rekhi, H. Kaur, K. Singh and A. K. Malik, *J. Fluoresc.* 2022, **32,** 1171-1188.